

ADVANCED FFAG OPTICS, DESIGN AND EXPERIMENT*

J.-B. Lagrange[†], Y. Mori,
Kyoto University Research Reactor Institute, Osaka, Japan

Abstract

Much progress has been made in the FFAG design with novel ideas, for example, FFAG straight line, FFAG with race track shape, FFAG with vertical orbit excursion, etc. Some of these were demonstrated experimentally. The talk will review the recent progress around the world.

INTRODUCTION

FFAG accelerators have been designed only in a circular shape, with horizontal excursion until recently, and zero-chromaticity is obtained with the vertical magnetic field B in the mid-plane following the so-called “scaling law” [1]

$$B = B_0 \left(\frac{r}{r_0} \right)^k \cdot \mathcal{F}, \quad (1)$$

with r the radius, r_0 the reference radius, k the constant geometrical field index, \mathcal{F} an arbitrary azimuthal dependent function and $B_0 = B(r_0)$. It constrains the transverse motion, since the machine can only be in a circular shape, and the excursion in the horizontal direction. Recent developments give the possibility to drive particles with no overall bend in FFAGs while keeping zero-chromaticity [2], and vertical excursion FFAGs are investigated these days [3, 4]. Fixed frequency acceleration has also been experimentally demonstrated.

This paper mainly reports on the straight FFAG line, theoretically and experimentally. Other recent developments are then briefly mentioned.

ZERO-CHROMATIC FFAG STRAIGHT LINE

Theory

The motion of a charged particle with a given momentum is described by the following linearized equations for small amplitudes

$$\begin{cases} \frac{d^2x}{ds^2} + \frac{1-n}{\rho^2}x = 0, \\ \frac{d^2z}{ds^2} + \frac{n}{\rho^2}z = 0, \end{cases} \quad (2)$$

in the local curvilinear coordinate system (x, s, z) . The field index n is defined as:

$$n = -\frac{\rho}{B} \left(\frac{\partial B}{\partial x} \right)_{\perp}, \quad (3)$$

with B the vertical component of the magnetic field. The symbol \perp means that the partial derivative is done in the

machine mid-plane perpendicularly to the closed orbit, and evaluated at $x = 0$. A necessary and sufficient condition of the invariance of the betatron oscillations along the curves $s = \text{const.}$ is

$$\begin{cases} \left(\frac{\partial \rho}{\partial p} \right)_s = 0, \\ \left(\frac{\partial n}{\partial p} \right)_s = 0. \end{cases} \quad (4)$$

From Eq. 4, since the curvature radius ρ does not depend on momentum, the similarity of the reference trajectories is a necessary condition for the invariance of the betatron oscillations. In the cartesian coordinates (X, Y, z) , it leads to

$$X_{co}(p, s) = \chi(p) + g(s), \quad (5)$$

where g is independent of momentum and can be seen as the “shape term”, common of all the reference trajectories, while χ is the “translation term”.

We now focus on the invariance of the field index n with momentum. If we derive in the median plane the equation $p = qB\rho$, for a particle of momentum p and charge q , with respect to x and at $x = 0$, we have:

$$B \left(\frac{\partial \rho}{\partial x} \right)_{\perp} + \rho \left(\frac{\partial B}{\partial x} \right)_{\perp} = \frac{1}{q} \left(\frac{\partial p}{\partial x} \right)_{\perp}. \quad (6)$$

The field index n can thus be rewritten as:

$$n = \left(\frac{\partial \rho}{\partial x} \right)_{\perp} - \frac{\rho}{p} \left(\frac{\partial p}{\partial x} \right)_{\perp}. \quad (7)$$

The field index n can then be expressed in the coordinates (χ, s, z) :

$$n = \left(\frac{\partial \chi}{\partial x} \right)_{\perp} \left[\left(\frac{\partial \rho}{\partial \chi} \right)_s - \rho m \right] + \left(\frac{\partial s}{\partial x} \right)_{\perp} \left(\frac{\partial \rho}{\partial s} \right)_x, \quad (8)$$

with m a parameter defined by:

$$m(\chi, s) = \frac{1}{p} \frac{dp}{d\chi}. \quad (9)$$

The parameter m can be rewritten with the magnetic field B as the normalized field gradient

$$m = \frac{1}{B} \frac{dB}{d\chi}. \quad (10)$$

The normalized field gradient m is independent of s , since the momentum is independent of s .

Since ρ does not depend on momentum, it does not depend on χ either:

$$\begin{cases} \left(\frac{\partial \rho}{\partial \chi} \right)_s = 0, \\ \left(\frac{\partial \rho}{\partial s} \right)_x = \frac{d\rho}{ds}. \end{cases} \quad (11)$$

* work supported by Japan Science and Technology Agency

[†] lagrange@rri.kyoto-u.ac.jp

Geometrical considerations [2] give that the field index can be rewritten as

$$n = -\rho (\cos \varphi + \sin \varphi \tan (\zeta + \varphi)) \cdot m + \frac{d\rho}{ds} \tan(\varphi + \zeta), \quad (12)$$

with φ the angle between the horizontal cartesian vector $u_{\vec{X}}$ and the vector \vec{x} , and ζ the angle between $u_{\vec{X}}$ and the line $s = \text{const.}$

Since n is independent of momentum along the curves $s = \text{const.}$, we can express the normalized field gradient $m(\chi, s)$ with Eq. 12:

$$m(\chi) = m_1 + m_2 \tan \zeta, \quad (13)$$

with m_1 and m_2 parameters independent of momentum:

$$\begin{cases} m_1 = \frac{1}{\rho} \left(\frac{d\rho}{ds} \sin \varphi - n \cos \varphi \right) \\ m_2 = \frac{1}{\rho} \left(\frac{d\rho}{ds} \cos \varphi + n \sin \varphi \right) \end{cases}. \quad (14)$$

Concerning the curves $s = \text{const.}$, they must be chosen continuous and at least two times differentiable. Their longitudinal variation must also fulfill the condition that the closed orbits never cross each other. Once the curve $s = 0$ is chosen, the similarity provides that every curve $s = \text{const.}$ follows the same law but for a constant.

The angle ζ is chosen independent of X , i.e. the curves $s = \text{const.}$ follow a tilted straight line:

$$Y_{s=\text{const.}}(X) = (X - X_0) \tan \zeta + Y_{s=\text{const.},0}, \quad (15)$$

with $Y_{s=\text{const.},0} = Y_{s=\text{const.}}(X_0)$. The particular case where the angle ζ is null leads to the rectangular case, since the curves $s = \text{const.}$ are perpendicular lines (see Fig. 1).

With the angle ζ independent of momentum, $m = m_1 + m_2 \tan \zeta$ is constant, and the momentum follows:

$$p = p_0 e^{m(\chi - \chi_0)}. \quad (16)$$

Furthermore, it would be interesting to write this expression in cartesian coordinates. Since we have from Eq. 5

$$\chi - \chi_0 = X_{co}(s, p) - X_{co}(s, p_0), \quad (17)$$

we can conclude that

$$X_{co}(s, p) = X_{co}(s, p_0) + \frac{1}{m} \cdot \ln \left(\frac{p}{p_0} \right). \quad (18)$$

The magnetic field distribution follows in cartesian coordinates

$$B(X, Y) = B_0 e^{m(X - X_0)} \mathcal{F}(Y - (X - X_0) \tan \zeta). \quad (19)$$

Experiment

The experiment aims to verify the zero-chromaticity of the straight scaling FFAG law by measuring the horizontal phase advances of two different energies.

The straight scaling FFAG experiment is performed in the accelerator complex of Kyoto University Research Reactor Institute, in Osaka, Japan.

The main components of this experiment are

FM cyclotrons and scaling FFAGs

No Sub Class

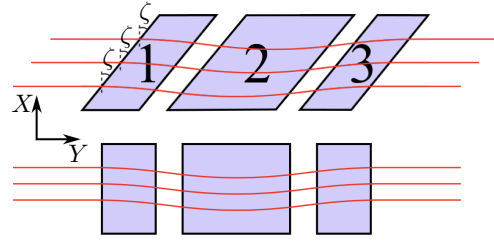


Figure 1: Tilted cell with constant angle (top). The magnets 1 and 3 are not identical to keep the same effective path for the particle. The rectangular case (bottom) is the particular case where the tilt angle is nul.

1. the H^- Linac injector of the 150 MeV FFAG complex, delivering 7 MeV and 11 MeV kinetic energy H^- particles collimated with 2 collimators,
2. a Courant-Snyder parameter measurement system,
3. the prototype of the straight scaling FFAG cell.

A schematic view of the setup is presented in Fig. 2. In this figure, the reference trajectory of the particles is plotted in red, and the straight FFAG cell in blue. Two collimators are installed before the straight cell to set the Courant-Snyder parameters. The Courant-Snyder parameters measurement system is added after the straight cell to determine the beam parameters at the exit.

The size of the collimators and the distance between them determine the Courant-Snyder parameters and the emittance at the entrance. The emittance ϵ is a function of the collimator size and the distance between the two collimators. If we backtrack the beam at the center of the collimator system, the beta-function is half of the distance between the two collimators and $\alpha = 0$. Size of the collimators has however to be small compared with the incident beam size. The collimator aperture has been set at 2 mm and the distance between the two collimators is set to 1530 mm. The 100% emittance is assumed to be 9 times the rms emittance. We then have at the entrance of the system

$$\begin{aligned} \epsilon_{100\%} &= 1.3 \pi \text{ mm.mrad}, \\ \epsilon_{rms} &= \frac{\epsilon_{100\%}}{9} = 0.14 \pi \text{ mm.mrad}, \\ \beta &= 0.77 \text{ m}, \\ \alpha &= 0. \end{aligned} \quad (20)$$

The Courant-Snyder parameter measurement system used in this experiment is similar to the emittance measurement “slit-grid method” [5], but with the grid replaced by a fluorescent screen. The slit is used to measure the horizontal angle of the beam, and the slope of the line x' vs. x . When the slit is removed, the size of the beam on the screen fitted with a gaussian gives access to the beta function value, and the center of the gaussian is taken as the position of the beam.

Since the width of the slit is crucial for the accuracy of the measurement, a slit of 0.1 mm width has been manufactured and used in the system.

ISBN 978-3-95450-128-1

121

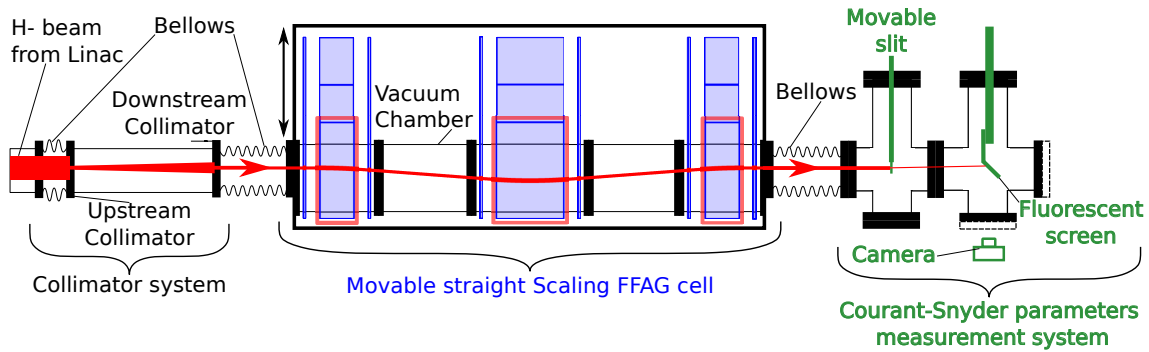


Figure 2: Schematic view of the straight scaling FFAG experiment.

Since the cell must be able to move in X direction to match the different trajectories without changing the magnetic field, it is installed on a ball-bearing system. Bellows before and after the cell allows the vacuum chamber to move along with the magnets without breaking the vacuum. The prototype for the straight scaling FFAG cell is a FDF triplet. Since the straight cell must move to match the different reference trajectories, one must limit the maximum necessary displacement. To that end, one would prefer to have a small dispersion, and m -value of the cell has been chosen to be 11 m^{-1} . The displacement between 11 MeV reference trajectory and 7 MeV reference trajectory is then around 2 cm. The parameters of the cell are summarized in Table 1.

Table 1: Parameters of the Straight Cell

Type	FDF
m -value	11 m^{-1}
Total length	4.68 m
Length of F magnet	15 cm
Length of D magnet	30 cm
Max. B Field (D magnet)	0.3 T
Max. B Field (F magnet)	0.2 T
Horizontal phase advance	87.7 deg.

A “C” type magnet has been chosen to have an easier access to the pole for field measurement. The minimum full gap size has been chosen to be 2.3 cm, to limit the ampere turns. Field clamps with 12 mm thickness have been adjusted at 60 mm from the poles to match the fringe field of the field model. The pole shape has been designed first in 2 dimensions with the finite element computation software POISSON [6], then it has been optimized in 3 dimensions with TOSCA code [7].

Concerning the coils, the current density is 2.7 A/mm^2 in the F magnets, and 4.4 A/mm^2 in the D magnet, and indirect water cooling has been chosen. The total power consumption of the three magnets is around 1 kW.

To check the manufacturing precision and have tracking in measured field maps, measurement of the field has been done. A 3-dimensional magnetic probe is controlled by the system YAMAHA RCX 142 series. The three magnets are



Figure 3: Picture of the straight scaling FFAG magnets prototype.

first aligned with a theodolite, then the probe is aligned according to the magnet system. Each magnet is measured separately.

The field is measured on 3 vertical layers: in the mid-plane ($z = 0$), $z = +5 \text{ mm}$ and $z = -5 \text{ mm}$. Each plane is measured in the good field region, with a horizontal step size of 5 mm, and a longitudinal step size of 10 mm. Drift space of 20 cm from both sides of each magnet are added to the effective field boundaries to measure the fringe fields.

Particle tracking in field model has been first done with a code based on Runge-Kutta integration developed at Kyoto University. Field follows the straight scaling law in the rectangular case, and fringe fields have linear fall-offs. The horizontal phase advance is constant and is equal to 87.7 deg. Tracking has then been done in field maps from TOSCA. The interpolation of the field between the map nodes is done linearly in 3 dimensions. The local horizontal phase advances in the Straight Cell are plotted in Fig. 4. The local normalized field gradient in the cell (or local m -

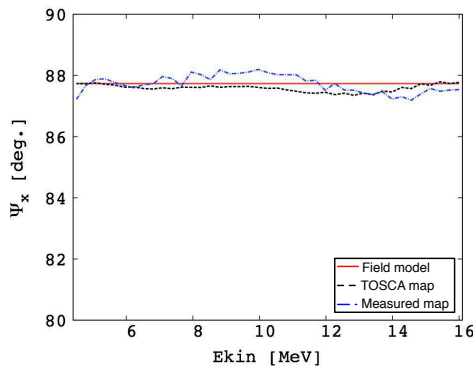


Figure 4: Horizontal local phase advances versus kinetic energy in the Straight FFAG line with field model (red plain line), with TOSCA field map (black dashed line) and with measured field maps (blue mixed line).

value) is defined from Eq. 18 as

$$\begin{cases} m(X_i) = \ln \left[\frac{\int B_z(X_i, Y) dY}{\int B_z(X_{ref}, Y) dY} \right] \cdot \frac{1}{X_i - X_{ref}}, \\ m(X_{ref}) = \frac{m(X_{ref-1}) + m(X_{ref+1})}{2}, \end{cases} \quad (21)$$

with $\int B_z(X_i, Y) dY$ the integral of the vertical magnetic field of the straight scaling FFAG cell along a straight line longitudinally at a constant horizontal abscissa X_i in the mid-plane. The resulting curve is presented in Fig. 5. The variation in the local m -value is so small that the variation in the horizontal phase advance is negligible. Particle tracking has finally been done in the measured field map. The horizontal local phase advances and local m -value in measured field map are shown in Fig. 4 and in Fig. 5, respectively. The agreement with the TOSCA tracking is within 1% for the m -value and for the horizontal phase advances.

The goal of this experiment is to measure the horizontal phase advance for 7 MeV and 11 MeV in the straight scaling FFAG cell prototype. To achieve this, the Courant-

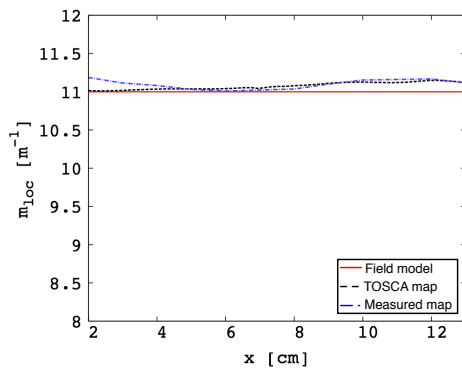


Figure 5: Local m -value versus horizontal abscissa in the Straight FFAG line in the good field region with field model (red plain line), with TOSCA field map (black dashed line) and with measured field maps (blue mixed line).

Snyder parameters as well as position and angle of the beam is measured at the exit of the Straight Cell when it is launched off its reference trajectory. The linear phase advance ψ can be calculated from:

$$\tan \psi = -\alpha_1 - \frac{\beta_1 x'_1}{x_1}. \quad (22)$$

with x_1 and x'_1 the distance and the angle to the reference trajectory at the exit of the cell, respectively, while α_1 , β_1 are the Courant-Snyder parameters at the exit of the cell, i.e. at the screen.

The result of the experiment consists of 6 series of data, taken at a different magnet position. The first position magnet corresponds to the reference trajectory position, from which the Courant-Snyder parameters are extracted. Then the position +10 mm and the position -10 mm give the angle and position of the beam off the reference trajectory. The second order of the dependance in amplitude of the phase advance is canceled by adding the 2 results. To have more statistical data, Courant-Snyder parameters are extracted from all magnet positions. Data consist of pictures of the fluorescent screen with different slit positions.

The alignment of the screen with the collimators is done with H^0 particles. The picture of the screen with the slit at the central position (aligned with a theodolite) is used to determine the reference point of the picture. Since an H^0 beam is present at the screen, the collimator system is installed off the mid-plane to separate the two beams at the screen, using the vertical betatron oscillation. It is then possible to detect the H^- beam at the screen without being disturbed by the H^0 beam. The angle of the beam x' can be obtained from the position at the screen and the position of the slit. The pictures without slit fitted by a gaussian can give the rms beam size at the screen. Assuming the geometrical emittance from the collimator system, we can thus get the beta function at the screen. The slope c of the line $x' - x'_0 = c(x_{slit} - x_{slit0})$ is the ratio of the Courant Snyder parameters α/β at the slit. By tracking in the drift space between the slit and the screen, we can get the alpha parameter at the screen. The resulting phase advances are presented in Table 2. We then have a difference of 1.6% between the two energies. There is no difference of phase advance with TOSCA tracking in the 11 MeV case, and the difference is 1.7% for the 7 MeV case. This good agreement clarifies the straight scaling law.

The errors are statistical and independent. They are evaluated from the beta function error (due to the fluctuation of the beam size). It affects both the Courant Snyder pa-

Table 2: Phase Advance ($\psi_{exp.}$) at the Screen in the Straight Scaling FFAG Experiment and Tracking Phase Advance ψ_{track} in TOSCA Field Map

	$\psi_{exp.}$ (deg)	ψ_{track} (deg)
11 MeV	87.5 ± 3.3	87.5
7 MeV	86.1 ± 9.6	87.6

rameters β_1 and α_1 at the slit, since α_1 is evaluated from the value of β_1 . It is 3.7% for 11 MeV, and 11.1% for 7 MeV. The incident beam fluctuates, especially for the 7 MeV case, degrading the emittance quality. It affects the beam size at the screen, with an error three times bigger than in the 11 MeV case. Since the cause of the error is from the incident beam, it is inevitable to have a large error for 7 MeV.

FFAG INSERTIONS

Combination of Scaling FFAG Cells

Two different FFAG cells can be combined by matching the dispersion [8]. The periodic beta-functions of the cells have also to be matched to limit the amplitude of the betatron oscillations. If a correct matching is not achievable, then a transparent insertion with a phase advance multiple of 180 deg. can be done for one of the two different types of cells.

Dispersion Suppressor

A principle of a dispersion suppressor in scaling FFAGs is presented in Fig. 6. The components of this scheme are three types of scaling FFAG cells. The area 1 contains FFAG cells with a dispersion D_1 at the border, the area 2, constituting the dispersion suppressor itself, contains FFAG cells with a dispersion D_2 at the borders, and the area 3 contains FFAG cells with a dispersion D_3 at the border. The conditions to have a dispersion suppressor are a phase advance of 180 deg. for the cells of the area 2 and the dispersion D_2 is half of the sum of D_1 and D_3 . This principle is based on the linear theory, so is valid as long as the effect of non-linearities is negligible. The amplitude detuning can break the zero-chromaticity if the difference of dispersion is too large regarding the momentum range.

One solution to overcome this problem is to reduce the dispersion with several dispersion suppressors. For n dispersion suppressors in cascade to go from an initial dispersion D_{ini} to a final dispersion D_{fin} , the periodic dispersion D_i of the dispersion suppressor number i must then follow

$$D_{ini} + (-1)^{n+1} D_{fin} = 2 \sum_{i=1}^n (-1)^{i+1} D_i. \quad (23)$$

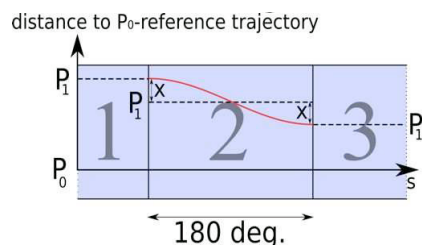


Figure 6: Principle of a dispersion suppressor with scaling FFAG cells.

VERTICAL FFAG

Excursion in FFAGs can be also done in the vertical direction. It has been first proposed by T. Ohkawa [9] in 1955 as an “electron cyclotron”. It has been rediscovered recently [3, 4]. In this case, the zero-chromaticity condition can be obtained with an exponential increase in the vertical direction. Vertical FFAG could be an asset when it comes to accelerate ultra-relativistic particles, because of its quasi-isochronicity.

FIXED FREQUENCY ACCELERATION

Some developments have also been done in FFAG acceleration. Serpentine acceleration in scaling FFAGs [10] and harmonic number jump acceleration [11] allow a fixed RF frequency acceleration in scaling FFAGs. Serpentine acceleration has been demonstrated theoretically and experimentally.

CONCLUSION

There has been a strong revival in FFAGs in the last years. Recent development in optics for zero-chromatic FFAGs, with straight lines, vertical excursion lead to new ring shapes and the introduction of insertions. Fixed RF frequency acceleration becomes also possible in zero-chromatic FFAGs. It opens a new range of applications for this type of machine.

AKNOWLEDGEMENTS

The authors would like to thank Dr. Y. Ishi, Dr. T. Ue-sugi and Dr. Y. Kuriyama, KURRI, for their valuable help in the straight experiment.

REFERENCES

- [1] K. R. Symon, D. W. Kerst, L. W. Jones, L. J. Laslett, K. M. Terwilliger, Fixed-Field Alternating-Gradient Particle Accelerators, Phys. Rev. 103 (6) (1956) 1837–1859.
- [2] J.-B. Lagrange et al, “Straight scaling FFAG beam line”, Nucl. Instr. Meth. A, vol. 691, pp. 55–63, 2012.
- [3] S. Brooks, Proc. of IPAC10, 2010.
- [4] S. Brooks, Proc. of IPAC11, 2011.
- [5] P. Fork, Lecture notes on beam instrumentation and diagnostics, Joint Universities Accelerator School, 2007.
- [6] L. A. A. C. Group, POISSON/SUPERFISH reference manual, Los Alamos National Laboratory, 1987.
- [7] Vector Fields Ltd., TOSCA OPERA-3D reference manual.
- [8] J.-B. Lagrange, “Study of zero-chromaticity in FFAG accelerators”, doctoral thesis, 2012.
- [9] T. Ohkawa, JPS meeting, 1955.
- [10] E. Yamakawa et al, “Serpentine acceleration in zero-chromatic FFAG accelerators”, Nucl. Instr. Meth. A, vol. 716, pp. 46–53, 2013.
- [11] T. Planche et al, “Harmonic number jump acceleration of muon beams in zero-chromatic FFAG rings”, Nucl. Instr. Meth. A, vol. 632, pp. 7–17, 2011.